Bioprocess Engineering 13 (1995) 161–169 © Springer-Verlag 1995

Modeling of heat and mass transfer for solid state fermentation process in tray bioreactor

S. Rajagopalan, J.M. Modak

Abstract A mathematical model is developed to simulate oxygen consumption, heat generation and cell growth in solid state fermentation (SSF). The fungal growth on the solid substrate particles results in the increase of the cell film thickness around the particles. The model incorporates this increase in the biofilm size which leads to decrease in the porosity of the substrate bed and diffusivity of oxygen in the bed. The model also takes into account the effect of steric hindrance limitations in SSF. The growth of cells around single particle and resulting expansion of biofilm around the particle is analyzed for simplified zero and first order oxygen consumption kinetics. Under conditions of zero order kinetics, the model predicts upper limit on cell density. The model simulations for packed bed of solid particles in tray bioreactor show distinct limitations on growth due to simultaneous heat and mass transport phenomena accompanying solid state fermentation process. The extent of limitation due to heat and/or mass transport phenomena is analyzed during different stages of fermentation. It is expected that the model will lead to better understanding of the transport processes in SSF, and therefore, will assist in optimal design of bioreactors for SSF.

List of symbols

$a_s(t)$	Transient interfacial area per unit volume for mass transfer, m^{-1}
A	Area of the bed, m^2
C_{O_2}	Gas phase oxygen concentration in the bed, kg/m^3
$C^f_{O_2}$	Film phase oxygen concentration, kg/m^3
C_p	Heat capacity, cal/(kg)(°C)
$D^b_{O_2}$	Effective diffusivity of oxygen in film, m^2/h
$D^b_{O_{2o}}$	Bi-molecular diffusivity of oxygen, m^2/h
$D^b_{O_2}(t)$	Transient effective diffusivity of oxygen in bed, m^2/h
ΔH	Heat of the reaction, cal/kg Cell
h	Convective heat transfer coefficient, cal/(m^2)(h)(°C)
H	Separation coefficient
k	Thermal conductivity, cal/(m)(h)(°C)
K_g	mass transfer coefficient, m/h
K_{O_2}	Saturation parameter for oxygen, kg/m^3
L	Height of the bed, m
n	Number of particles per unit volume of bed
r	Radial position coordinate, m
r_x	Cell mass production rate, kg cell mass/m^3
$R(t)$	Transient radial position coordinate, m
R_c	Particle radius, m
R_i	Initial biofilm radius, m
R_{max}	Maximum biofilm radius, m
t	time, h
T	Temperature, °C
X	Biomass concentration, kg cell/m^3
X_{max}	Maximum biomass concentration, kg cell/m^3
X^p	Biomass, kg cell
y	Vertical position coordinate, m
$Y_{O_2/X}$	Oxygen yield coefficient, kg O_2/kg Cell
z	Transformed radial position coordinate

Greek letters

ε	Porosity of the bed
ρ_s	Apparent density of the substrate, kg/m^3
ρ_x	Density of the fungal cell, kg/m^3
τ	Tortuosity of the bed
$\mu_m(T)$	Maximum growth rate, 1/h

Received 12 October 1994

S. Rajagopalan, J.M. Modak
Department of Chemical Engineering, Indian Institute of Science, Bangalore 560012, India

Correspondence to: J.M. Modak

1 Introduction

Solid state fermentation (SSF) is defined as any fermentation in which the substrate is not a free liquid [1]. The SSF involving growth of microorganisms on moist solid substrate has received a great deal of attention in recent years because of a number of advantages associated with SSF over submerged fermentation [9]. Many experimental investigations for production of enzymes, organic acids and alcohols by SSF have appeared in literature. The static tray bioreactor, also known as koji bioreactor, is the commonly used bioreactor for SSF. In SSF, bacterial and yeast cultures grow on the surface of the solid substrate while filamentous fungi are able to penetrate the solid [12]. It has been observed during the fungal growth that a loose mycelial structure (biofilm) develops around the solid particle and the thickness of the biofilm increases as growth occurs. The growth of the microorganism ceases once the cell density approaches its limiting value, normally in the range of 10–30 kg/m^3 of bioreactor volume. Several factors are responsible for limiting the growth of microorganism in SSF. Laukevics et al. [11] reported that steric hindrance, which is a combined effect of geometric limitation on growth in void spaces of substrate bed, limitations of mass transfer and substrate availability, is partially responsible for limiting cell

growth. The heat build-up due to exothermic nature of growth processes is the second important factor determining the extent of growth in SSF. Indeed, Rathbun and Shuler [17] reported steep temperature gradients inside the static bioreactor with temperatures inside the bed reaching 50 °C which are sufficient for preventing further growth of microorganisms. Many of these growth processes being aerobic, the limitation of oxygen transfer from bulk to the interiors of the static moist bed of solids contributes further to the growth limitations. The interaction between these complex heat and mass transfer phenomena often leads to development of steep concentrations and temperature gradients which results in inhomogeneous conditions in the bioreactor, and therefore, inefficient utilization of the bioreactor capacity. A detailed knowledge of the inter-relationship of heat and mass transfer with mold growth kinetics is essential for the rational design and control of solid state fermentations.

The reported literature on SSF primarily deals with experimental investigations with different microorganisms and substrate but very little attention has been paid to quantitative understanding of the growth processes in SSF. The models incorporating mass transfer limitations for describing growth of pellets in submerged liquid [10] or growth on the surface of semi-solid agar matrix [8, 13] are not applicable for SSF processes, in particular for describing growth in bed of moist solid substrate particles. Finger et al., [5] developed a conceptual model to predict the rate of break down of semisolid cellulosic material and to predict oxygen and temperature distribution in a compost pile. However, the authors did not consider the growth of microorganisms. Saucedo-Castaneda et al., [18] developed a model to evaluate the heat transfer effects in a static cylindrical bioreactor without considering oxygen transfer limitations. Recently, Raghava Rao et al. [15] proposed a model for the prediction of oxygen profiles in an isothermal static tray bioreactor. According to classification of Froment and Bischoff [7], all the above mentioned models can be termed as pseudohomogenous in which the solid (biofilm) phase is not explicitly accounted for. In our previous work, a psuedohomogenous model for oxygen transfer in solid state fermentation process in an nonisothermal tray bioreactor was reported [16].

The objective of this work is to present a model for heat and mass transfer processes accompanying the growth of microorganism in static tray bioreactor with oxygen as the single growth limiting substrate. A heterogeneous model is developed by writing separate conservation equations for fluid (oxygen) and solid phase. The solid phase consists of the moist solid substrate with expanding biofilm around solid substrate. Some analytical results on growth of biofilm on individual solid substrate particles are presented first. The simulation results for static tray bioreactor consisting of bed of solid substrate particles are presented next. The growth of Aspergillus niger on moist wheat bran particles is chosen as model system.

2
Development of the model

The model is developed taking into consideration various typical features of static tray bioreactor which is schematically

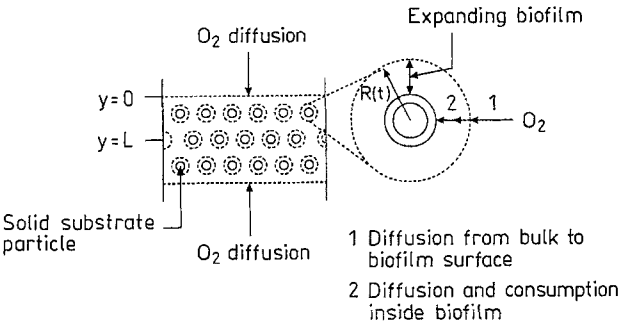

Fig. 1. Schematic representation of tray bioreactor for solid state fermentation process

shown in Fig. 1. The bioreactor is packed with moist solid substrate particles of radius R_c and the bed of solids of height 2L is supported by a perforated plate enabling transfer of oxygen from the top as well as bottom of the bed. The growth of microorganism and the heat and mass transfer processes accompanying the growth are visualized as follows. The bioreactor is inoculated with microorganism and a biofilm of radius R develops around the substrate particle. Air flows across the top and bottom of moist solid bed. The oxygen from air diffuses through the void spaces of the bed and gets transferred across the gas-biofilm interphase. In the biofilm, there is simultaneous diffusion and consumption of oxygen which leads to growth of microorganism. As a result of growth, the biofilm expands or R increases as fermentation proceeds and void space in the bed decreases leading to reduction in oxygen diffusion in the bed. The heat liberated during the growth process leads to rise in temperature inside the bed which in turn affects the growth rate of the microorganism.

Several assumptions made for the development of the model are as follows:

1. Oxygen is the growth limiting substrate and other substrates are present in excess. The oxygen concentration on either side of the bed is constant and is equal to atmospheric concentration (0.28 kg/m^3).
2. Oxygen transferred to the film is consumed throughout the film and the oxygen consumption follows Monod's kinetics.
3. The dependence of the growth rate of microorganism on the temperature is nonmonotonic with growth rate being maximum at 38 °C and decreasing on either side.
4. The density of the fungal cell (ρ_z) is constant.

In view of the above mentioned assumptions, the unsteady state balance equations for oxygen concentration in void space in bed (C_{O_2}), oxygen concentation in the biofilm ($C^f_{O_2}$), cell mass around each particle (X^p) and temperature (T) are written as follows:

$$\frac{\partial(C_{O_2}\varepsilon(t))}{\partial t}=\frac{\partial}{\partial y}\left(D^b_{O_2}\frac{\partial C_{O_2}}{\partial y}\right)-K_g a_s(t)\,(C_{O_2}-HC^f_{O_2}|_{R(t)}), \quad (1)$$

$$\frac{\partial C^f_{O_2}}{\partial t}=\frac{D^f_{O_2}}{r^2}\frac{\partial}{\partial r}\left(r^2\frac{\partial C^f_{O_2}}{\partial r}\right)-\mu_m(T)\,\rho_x Y_{O_2/X}\frac{C^f_{O_2}}{(K_{O_2}+C^f_{O_2})}, \quad (2)$$

$$\frac{\partial X^p}{\partial t} = \int_{R_c}^{R(t)} \mu_m(T)\,\rho_x \frac{C^f_{O_2}}{(K_{O_2}+C^f_{O_2})}\,4\pi r^2\,dr, \tag{3}$$

$$\frac{\partial T}{\partial t} = \frac{k}{\rho_s C_p}\frac{\partial^2 T}{\partial y^2} + \frac{\Delta H}{\rho_s C_p} r_x, \tag{4}$$

where r_x is average growth rate of biofilm per unit volume of the bioreactor which can be obtained by multiplying the growth rate around each particle by number of particles (n) per unit volume of the bioreactor as follows:

$$r_x = n \int_{R_c}^{R(t)} \mu_m(T)\,\rho_x \frac{C^f_{O_2}}{(K_{O_2}+C^f_{O_2})}\,4\pi r^2\,dr. \tag{5}$$

A fifth degree polynomial is used for describing the effect of temperature on maximum specific growth rate ($\mu_m(T)$) of Aspergillus niger [18]:

$$\mu_m(T) = -11.3 + 1.95T - 0.13T^2 + 4.36x\,10^{-3}T^3 - 6.91x\,10^{-5}T^4 + 4.19x\,10^{-7}T^5. \tag{6}$$

The radius of the biofilm ($R(t)$) and the average cell density per unit volume of the bioreactor ($X(t)$) can be related to the cell mass around each particle X^p as follows:

$$X^p = \frac{4}{3}\pi\rho_x(R(t)^3 - R_c^3), \qquad X(t) = nX^p. \tag{7}$$

The diffusivity of O_2 in bed $D^b_{O_2}$, the porosity of the bed $\varepsilon(t)$, defined as the ratio of void volume of the total bioreactor volume and the interfacial area mass transfer $a_s(t)$, defined as surface area of the particles per unit volume of the bed, are related to the radius of the biofilm as follows:

$$D^b_{O_2}(t) = \frac{D^b_{O_{2o}}\varepsilon(t)}{\tau}, \quad \varepsilon(t) = 1 - n\frac{4}{3}\pi R(t)^3, \quad a_s(t) = n4\pi R(t)^2, \tag{8}$$

where τ is tortuosity factor [7].

Initial conditions for the above set of equations are:

$$t=0: \quad C_{O_2} = C_{O_{2o}} \quad C^f_{O_2} = C^f_{O_{2o}}; \quad X^p = X^p_o; \quad T = T_o. \tag{9}$$

Boundary conditions are, for all $t>0$;

$$y=0: \quad C_{O_2} = C_{O_{2o}}; \quad T = T_o \quad \text{and}$$

$$y=L, \quad \frac{\partial C_{O_2}}{\partial y} = 0; \quad \frac{\partial T}{\partial y} = 0, \tag{10}$$

and for all y:

$$r=R_c: \quad \frac{\partial C^f_{O_2}}{\partial r} = 0 \quad \text{and}$$

$$r=R(t), \quad K_g(C_{O_2} - HC^f_{O_2}|_{R(t)}) = D^f_{O_2}\left(\frac{\partial C^f_{O_2}}{\partial r}\right)_{R(t)}. \tag{11}$$

The above equations are nondimensionalised as follows:

$$\bar{t} = \frac{t\varepsilon(0)D^b_{O_2}}{L^2}; \quad \bar{y} = \frac{y}{L} \quad \bar{C}_{O_2} = \frac{C_{O_2}}{C_{O_{2o}}};$$

$$\bar{C}^f_{O_2} = \frac{C^f_{O_2}}{C^f_{O_{2o}}}; \quad \bar{X}^p = \frac{X^p}{X^p_0}; \quad \bar{T} = \frac{T}{T_o}.$$

Table 1. Parameters used in simulations

Constants	Value	Units	Reference
A	1	m^2	assumed
$C_{O_{2o}}$	0.28	kg/m^3	calculated
$C^f_{O_{2o}}$	6.08×10^{-3}	kg/m^3	10
C_p	320	cal/(kg)(°C)	14
$D^b_{O_2}$	2.8×10^{-3}	m^2/h	calculated
$D^f_{O_2}$	6.08×10^{-6}	m^2/h	10
ΔH	7×10^6	cal/kg cell	3
H	46	–	calculated
K_{O_2}	9.6×10^{-5}	kg/m^3	10
k	44	cal/(kg)(°C)(h)	14
$K_g a_s$	6.4	1/h	2
L	5×10^{-2}	m	calculated
n	1.07×10^7	$1/m^3$	calculated
R_c	2.5×10^{-3}	m	assumed
T_o	35	°C	assumed
X^p_o	5.71×10^{-10}	kg cell	assumed
X_{max}	30	kg/m^3	11
$Y_{O_2/X}$	3	kg O_2/kg cell	assumed
ρ_x	1000	kg/m^3	assumed
ρ_s	700	kg/m^3	assumed
$\varepsilon(0)$	0.3	–	assumed

The assumption of expanding biofilm implies that the interphase between the gas and biofilm phase is continuously changing with time or progress of the fermentation. As a result, the unsteady state model represented by Eqs. (1) through (4) is a set of two dimensional partial differential equations with moving boundary conditions. In order to handle moving boundary condition, the technique of immobilizing the moving front [4] is utilized with following transformation:

$$z(t) = \frac{r - R_c}{R(t) - R_c}, \tag{12}$$

so that when $r=R_c$; $z(t)=0$ and when $r=R(t)$; $z(t)=1$.

The dimensionless form of the model obtained using above mentioned transformations is a two dimensional problem, one in the y-direction (height of the bed) and the other in the z-direction (film thickness). Orthogonal collocation technique [6] in two dimensions has been used to discretize the spatial terms appearing in the equations and the resulting set of ordinary differential equations has been integrated using the IMSL routine DGEAR. Various kinetic parameters used for simulation along with its source are listed in Table 1.

3 Results and discussion

3.1 Cell growth around single particle

In this section, results for the growth of cell around single particle are presented in order to gain some insight into development of biofilm around individual particles. The solid substrate particle of radius R_c is assumed to be covered with the biofilm of initial radius R_i. As cells grow around the particle, the biofilm radius $R(t)$ increases. It is assumed that the gas phase oxygen concentration (C_{O_2}) and temperature (T) surrounding the biofilm is maintained at certain value.

Therefore, balance equation for film phase oxygen concentration ($C^f_{O_2}$) and cell mass surrounding each particle (X^p) are considered in this section. The analytical solution of these two balance equations can be obtained by making two assumptions. The first assumption required to get analytical results is the quasi-steady state assumption for film phase oxygen concentration. With this assumption, the mass balance equation for $C^f_{O_2}$ reduces to:

$$\frac{D^f_{O_2}}{r^2}\frac{\partial}{\partial r}\left(r^2\frac{\partial C^f_{O_2}}{\partial r}\right)=\mu_m(T)\rho_x Y_{O_2/X}\frac{C^f_{O_2}}{(K_{O_2}+C^f_{O_2})}, \quad (13)$$

with boundary conditions as before (Eq. (11)). The second assumption is regarding the rate of oxygen consumption. At very high values of $C^f_{O_2}$ ($C^f_{O_2} \gg K_{O_2}$), the oxygen consumption kinetics is zero order while at low values of $C^f_{O_2}$ ($C^f_{O_2} \ll K_{O_2}$) the kinetics is first order. The analytical solutions can be obtained for both zero order and first order kinetics.

3.1.1
Zero order kinetics

For zero order kinetics, Eq (13) along with boundary conditions (11) can be solved to yield the expression for variation of $C^f_{O_2}$ with biofilm radius r as follows:

$$C^f_{O_2}=\frac{C_{O_2}}{H}+\frac{\alpha}{6}(r^2-R^2)+\frac{\alpha R_c^3}{3}\left(\frac{1}{r}-\frac{1}{R}\right)-\frac{\alpha\beta}{3}\left(R-\frac{R_c^3}{R^2}\right), \quad (14)$$

where

$$\alpha=\frac{\mu_m(T)\rho_x Y_{O_2/X}}{D^f_{O_2}} \quad \text{and} \quad \beta=\frac{D^f_{O_2}}{K_g H}.$$

The relationship holds as long as $C^f_{O_2}$ is nonnegative, which will be true from $r=R$ inward to a critical radius $r=R^*$, determined by setting $C^f_{O_2}=0$ in Eq. (14). This yields:

$$\frac{C_{O_2}}{H}+\frac{\alpha}{6}(R^{*2}-R^2)+\frac{\alpha R_c^3}{3}\left(\frac{1}{R^*}-\frac{1}{R}\right)-\frac{\alpha\beta}{3}\left(R^*-\frac{R_c^3}{R^{*2}}\right)=0, \quad (15)$$

subject to the condition that $R^* \geq R_c^*$. Consequently, there is an interior portion of the biofilm (from $r=R_c$ to $r=R^*$) in which $C^f_{O_2}=0$ and there is no growth in this region (inactive cell mass). Only the outer region of the biofilm (from $r=R^*$ to $r=R(t)$) grows actively. Since biofilm is continuously expanding, R^*, which is the solution of Eq. (15), will also change with time. An interesting solution of Eq. (15) is the case in which R^* approaches R. This is a limiting case in which entire biofilm is devoid of oxygen, and therefore, cell growth or biofilm expansion will completely cease. Thus, substituting $R^*=R$ in Eq. (15) yields the maximum radius of the biofilm, R_{max} as determined by solution of Eq. (16):

$$\left(R_{max}-\frac{R_c^3}{R_{max}^2}\right)=\frac{3C_{O_2}K_g}{\mu_m(T)\rho_x Y_{O_2/X}}. \quad (16)$$

The maximum cell density of active biomass can be calculated by using relation $X_{max}=n\frac{4}{3}\pi\rho_x(R^3_{max}-R^3_C)$. Thus, oxygen transfer limitations, in particular external mass transfer limitations, can lead to stoppage of cell growth under conditions of zero order kinetics for oxygen consumption. It can be seen from Eq. (16) that R_{max} (or X_{max}) depend on the gas phase oxygen concentration (C_{O_2}) and temperature (T)

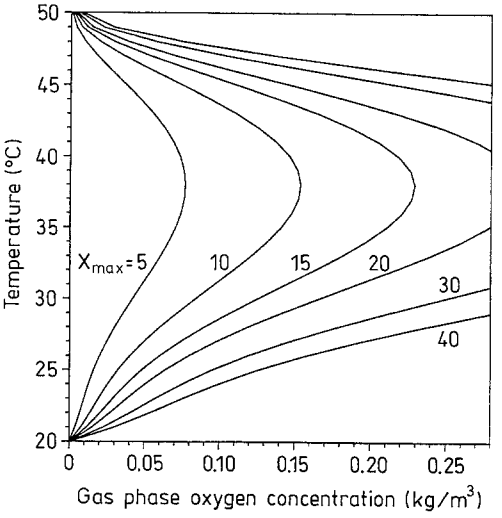

Fig. 2. Contours of maximum cell density (X_{max}) in phase plane of gas phase oxygen concentration and temperature surrounding the biofilm

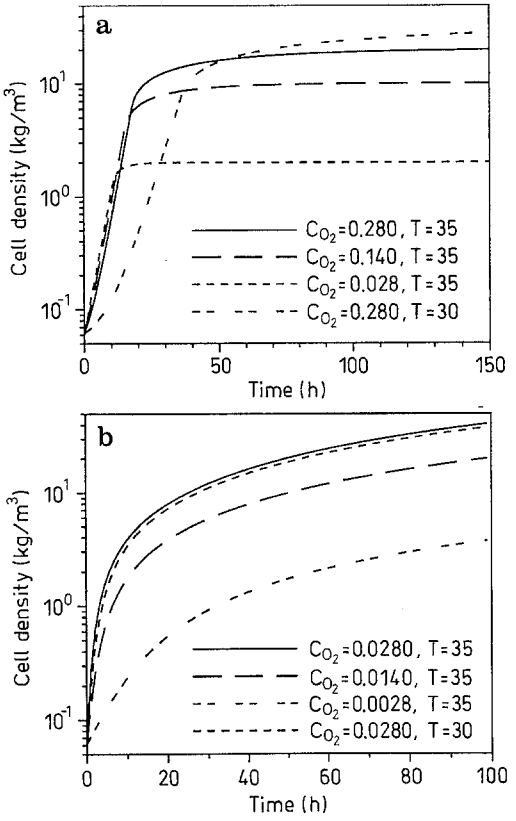

Fig. 3. Cell density variation with time for (**a**) zero order and (**b**) first order oxygen consumption kinetics

surrounding the biofilm. Fig. 2 shows the contours of X_{max} in phase plane of temperature and oxygen concentration in gas phase. At any given temperature X_{max} increases as gas phase oxygen concentration increases. At any given oxygen concentration, X_{max} first decreases as temperature is increased up to 38 °C but increases as temperature is further increased. This is because the growth rate of the cells is maximum at 38 °C. At fixed value of oxygen concentration, the cells consume the oxygen rapidly which result in lower values of

X_{max}. In case of growth of cells in tray packed with moist solid, both gas phase oxygen and temperature will vary along the height of the solid bed, and therefore, it can be expected that X_{max} will also vary along the height of the bed. Such variations have indeed been experimentally observed [18].

The variation of cell density with time can be calculated by incorporating zero order kinetics for oxygen consumption and changing the lower limit of integration from R_c to R^* in the cell mass balance Eq. (3) which yields:

$$\frac{dX^p}{dt} = \int_{R_c}^{R(t)} \mu_m(T)\rho_x 4\pi r^2 dr = \frac{4}{3}\pi\rho_x(R^3 - R^{*3}) = \mu_m(T)X^p\left(1 - \frac{X_i^p}{X^p}\right), \quad (17)$$

pointed out earlier. For fixed value of gas phase oxygen concentration (0.28 kg/m^3) and lower temperature (30 °C), the growth rate is lower during exponential phase as $\mu_m(T)$ is lower at 30 as compared to 35 °C. The time required for cell density to reach maximum value is prolonged, and therefore, the maximum density is higher at 30 °C as compared to that at 35 °C.

3.1.2 First order kinetics

For first order kinetics, Eq. (13) along with boundary conditions (11) can be solved to yield the expression for variation of $C_{O_2}^f$ with biofilm radius r as follows:

$$C_{O_2}^f = \frac{C_{O_2}R^2}{r}\frac{(\delta R_c + 1)e^{\delta(r-R_c)} + (\delta R_c - 1)e^{-\delta(r-R_c)}}{[HR + \gamma(\delta R - 1)](\delta R_c + 1)e^{\delta(R-R_c)} + [HR - \gamma(\delta R + 1)](\delta R_c - 1)e^{-\delta(R-R_c)}}, \quad (18)$$

where

$$X_i^p = \frac{4}{3}\pi\rho_x(R^{*3} - R_C^3)$$

is the inactive cell mass because of oxygen depletion. Fig. 3(a) shows cell density variations with time for various values of C_{O_2} and T. For $C_{O_2} = 0.28$ kg/m^3 and $T = 35$ °C, the cell density increases exponentially with time till about 20 hours. Since the biofilm thickness initially is small, the oxygen is present in the entire biofilm (R^*, solution of Eq. (15), is less than R_c) and the entire biofilm is actively growing ($X_i^p = 0$). As time progresses, the oxygen gets depleted in the interior of the biofilm (from $r = R_c$ to $r = R^* > R_c$) and part of the biofilm is inactive ($X_i^p > 0$). This results in reduction in cell growth rate (Eq. (17)) which can be seen between $t = 20$ to $t = 50$ h. At still higher times, the biofilm expands to the extent that oxygen is depleted practically in the entire biofilm, that is, R^* approaches R. In such cases, the entire biofilm is inactive ($X_i^p = X^p$) and growth ceases completely (Eq. 17)). Figure 3(a) shows this effect beyond 50 hours when cell density reaches the maximum limit for given value of C_{O_2} and T, and cell growth stops. It is interesting to note that cell growth behavior predicted by Eq. (17) is similar to that obtained using empirical logistic growth rate expression often used to account for the maximum limit of cell growth. It should be pointed out that such a limitation is not assumed a priori in the model but is predicted by the model as a result of oxygen transfer limitations. The cell growth profiles for fixed value of temperature (35 °C) and various values of gas phase oxygen concentration are also shown in Fig. 3(a). The growth profiles are similar for various values of C_{O_2} during exponential growth phase as growth rate is independent of oxygen concentration. However, the maximum cell density obtained varies with C_{O_2} as

where

$$\delta = \left(\frac{\mu_m(T)\rho_x Y_{O_2/X}}{D_{O_2}^f K_{O_2}}\right)^{1/2} \quad \text{and} \quad \gamma = \frac{D_{O_2}^f}{K_g}.$$

Unlike zero order kinetics, first order kinetics inplies that the oxygen consumption rate goes to zero as oxygen concentration goes to zero. As a result, the film phase oxygen concentration will never go to zero as long as the gas phase surrounding the film has some oxygen which can also be seen from Eq. (18). Therefore, model with first order kinetics does not predict the conditions of complete cell growth stoppage. In other words, biofilm will continue to expand unlike zero order kinetics where termination of biofilm expansion is predicted. However, the variation of cell density with time can be calculated by incorporating first order kinetics for oxygen consumption and using Eq. (13) along with boundary conditions (11) in the cell mass balance Eq. (3) which yields:

$$\frac{dX^p}{dt} = \int_{R_c}^{R(t)} \frac{\mu_m(T)\rho_x}{K_{O_2}} C_{O_2}^f 4\pi r^2 dr = 4\pi\frac{\mu_m(T)\rho_x}{K_{O_2}}\frac{1}{\delta^2}R^2\left(\frac{\partial C_{O_2}^f}{\partial r}\right)_{r=R}. \quad (19)$$

Rearrangement of Eq. (19), by evaluating $\left(\frac{\partial C_{O_2}^f}{\partial r}\right)_{r=R}$ from Eq. (18) and using the relation $X^p = \frac{4}{3}\pi\rho_x(R^3 - R_C^3)$, yields:

$$\frac{dR}{dt} = \frac{\mu_m(T)C_{O_2}}{K_{O_2}\delta^2}\frac{(\delta R - 1)(\delta R_c + 1)e^{\delta(R-R_c)} - (\delta R + 1)(\delta R_c - 1)e^{-\delta(R-R_c)}}{[HR + \gamma(\delta R - 1)](\delta R_c + 1)e^{\delta(R-R_c)} + [HR - \gamma(\delta R + 1)](\delta R_c - 1)e^{-\delta(R-R_c)}}. \quad (20)$$

Equation (20) is a first order differential equation in $R(t)$ which can be integrated along with initial condition $R=R_i$ at $t=0$. The cell density variations with time which is calculated using relation $X(t)=n\frac{4}{3}\pi\rho_x(R^3-R_C^3)$ are shown in Fig. 3(b). Since first order kinetics is likely to be present at low oxygen concentration, the simulations are done for low gas phase oxygen concentrations ($0.0028-0.028$ kg/m^3). For $C_{O_2}=0.028$ kg/m^3 and $T=35$ °C, the cell density increases exponentially with time till about 10 hours. Since the biofilm thickness initially is small, the film phase oxygen concentration with radius of the biofilm is very small $\left(C_{O_2}^f \approx \frac{C_{O_2}}{H}\right)$. In such case, cell mass balance Eq. (19) reduces to $\frac{dX^p}{dt}=\frac{\mu_m(T)\rho_x C_{O_2}}{K_{O_2}H}X^p$ which predicts exponential growth phase. As time progresses, the oxygen gets depleted in the interior of the biofilm (from $r=R$ to $r=R_c$) and steep gradients in film phase oxygen concentration develop. This results in reduction in cell growth rate (Eq. (20)) which can be seen after 10 hours. As fermentation proceeds, the growth rate decreases continually. The cell density increases, although with much slower rate, and never reaches the maximum limit which is observed in the case of zero order kinetics for oxygen consumption. The cell growth profiles for fixed value of temperature (35 °C) and various values of gas phase oxygen concentration are also shown in Fig. 3(b). The growth profiles are similar in nature for various values of C_{O_2} except the growth rates and the cell density obtained decreases as the gas phase oxygen concentration decreases.

The analysis of cell growth around single particle clearly shows that under conditions of zero order kinetics of oxygen consumption, there is an upper limit on the cell density that can be obtained. On the other hand, in case of first order kinetics, cell density continues to increase, although at slower rate, as long as oxygen in gas phase in not depleted. Zero and first order kinetics are the limiting cases of the Monod's kinetics assumed for the oxygen consumption. Monod's kinetics reduces to zero order kinetics when oxygen concentrations are high while it reduces to first order kinetics when oxygen concentrations are low. Thus, in case of cell growth following Monod's kinetics, the cell growth pattern will be similar to that obtained with zero order kinetics when (a) biofilm thickness is small and/or (b) gas phase oxygen concentrations are high. On the other hand, the cell growth with Monod's kinetics will be similar to that obtained with first order kinetics when (a) biofilm thickness is high and/or (b) gas phase oxygen concentration is low. As biofilm is expanding, the pattern of increase in biofilm radius will shift from pattern determined by zero order kinetics to that determined by first order kinetics. It can, therefore, be concluded that oxygen transfer limitations alone will not predict upper limit on cell density when oxygen consumption obeys Monod's kinetics.

3.2
Cell growth in tray bioreactor

Analysis of the previous section was aimed at investigating growth around single particle. The tray bioreactor consists of number of such particles packed in a bed. It is clear from earlier analysis that the cell growth around invidual particle is dependent on the gas phase oxygen concentration (C_{O_2}) and temperature (T) surrounding the particle. Both these quantities will vary as function of time as well as the bed height. Therefore, single particle analysis can not be simply extrapolated to predict the cell growth in tray bioreactor. In this section, the results of cell growth in a tray bioreactor packed with moist solid are presented. The problem, described by the balance Eqs. (1) thorough (4) with suitable initial (Eq. (9)) and boundary conditions (Eqs. (10) and (11)), is symmetric with respect to plane $y=L$, and therefore, the simulation results are presented only for top half of the bed, that, from top of the bed ($y=0$) to the center of the bed ($y=L$). As pointed out earlier, oxygen transfer limitations alone can not predict upper limit on cell growth. In order to take into account the experimental reality of upper limit of cell growth in solid state fermentations, it is assumed that the growth rate drops to zero as cell density approaches critical value X_{max}. Laukevics et al. [11] reported that due to stearic hindrences the maximum cell density attainable in solid state fermentation is in the range of 10–30 kg/m^3, and therefore, X_{max} is assumed to be 30 kg/m^3 in this study.

The transient temperature, gas-phase oxygen concentration and cell density profiles at different positions in the bed are presented in Figs. 4(a), (b) and (c), respectively. The temperature profiles in Fig. 4(a) show that the heat liberated during growth process increases the temperature in the bed and due to the heat transfer limitations, the center portions experience the maximum heat build up. During the initial stages of fermentation ($t=10$ h), the center regions of the bed experience better growth than the top regions because the temperatures inside are quite close to 38 °C at which the specific growth rate ($\mu_m(T$, Eq. (6)) is maximum. As fermentation proceeds ($t=20$, 30 and 40 h), the temperatures in the center portion are much higher as compared to that in

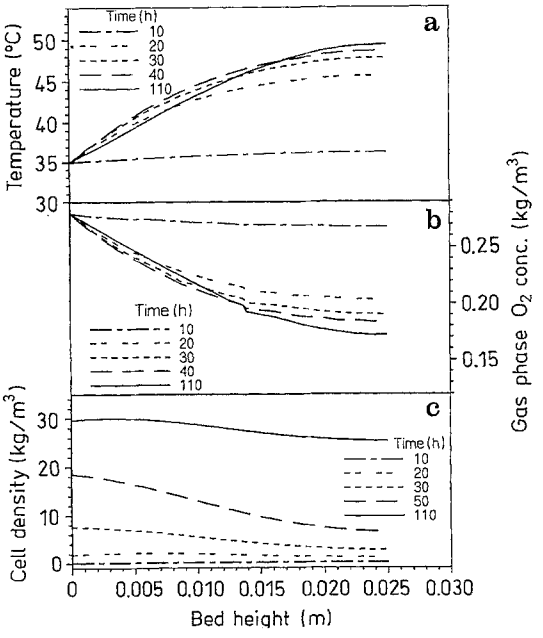

Fig. 4. (a) Temperature (b) gas phase oxygen concentration and (c) cell density profiles as a function of bed height at different fermentation times

the top region of the bed. Once the temperature crosses 38 °C, the corresponding portions of the bed experience a reduction in growth rate. At 110 hours, growth stops at the top regions (from $y=0$ to $y=0.01$) of the bed because the cell mass reaches the maximum attainable value, Fig. 4(c). Hence there is no more production of heat in those zones and it can be seen from Fig. 4(a) that temperature in this zone is reduced. The inner regions are still actively growing and producing heat and hence the temperature in the center regions are high.

The profiles of oxygen concentration in the bed with time given in Fig. 4(b) show that the supply of oxygen from the top of the bed is enough to keep the region near the top of the bed very well saturated with oxygen. The entire bed is assumed to be saturated with oxygen initially and the consumption of oxygen is low in the initial stages of fermentation ($t=10$ h). Therefore, the gas phase concentration is more or less uniform a cross the bed at $t=10$ h. As fermentation proceeds ($t=20$, 30 and 40 h), there is rapid consumption of oxygen throughout the bed. Since the availability of oxygen in the center is limited by oxygen transfer through the bed, the region near the center of the bed experiences lower concentrations of oxygen. As a result steep oxygen concentration gradients develop and gas phase oxygen concentration decreases from the top of the bed to the center of the bed. At 110 hours, growth stops at the top regions (from $y=0$ to $y=0.01$) of the bed because the cell mass reaches the maximum attainable value (Fig. 4(c)). Therefore, oxygen concentration in the top region increase at 110 h as compared to $t=40$ h. Since the cells in the center region are still actively growing, there is further drop in oxygen concentration in this region.

Cell mass variations as a function of bed height at various times given in Fig. 4(c) reveal that during the initial stages of feremention ($t=10$ and 20 h), the cell density is more or less uniform across the entire bed. However, as fermentation progresses ($t=30$ and 50 h), the cell growth is nonuniform across the bed as a result of temperature and oxygen concentration gradients in the bed. The temperature increases and oxygen concentration decreases from top to the center of the bed. Both these factors lead to reduction in growth rate at the center of the bed as compared to the top region. At 110 hours, maximum attainable cell mass (30 kg/m^3) is obtained only near the top region (from $y=0$ to 0.01 m) of the bed. The cell mass in the interior portion remains below 30 kg/m^3 implying that the bed is not efficiently utilized due to poor design. The biofilm thickness ($R(t)-R_c$) at 110 hours near the top region is approx. 350 microns. This is the characteristic radial increase in the particle sizes observed in solid state fermentation [11].

Perhaps more interesting trends are the oxygen concentration profiles in the biofilm around the particles. Though attempts have been made to measure oxygen concentrations in the case of Aspergillus niger pellets [10, 19], no such effort has so far been made in the case of the film around the solid particles. The diffusivity of oxygen in the film can become the deciding factor in making oxygen available for the aerobic growth of fungi and such factors can be studied in the present model. The film phase oxygen profiles are at different times, $t=15$, 25, 40, and 76 h, are shown in Figs. 5(a), (b), (c) and (d), respectively. Since the cell growth behavior is different at different bed heights, the film phase oxygen

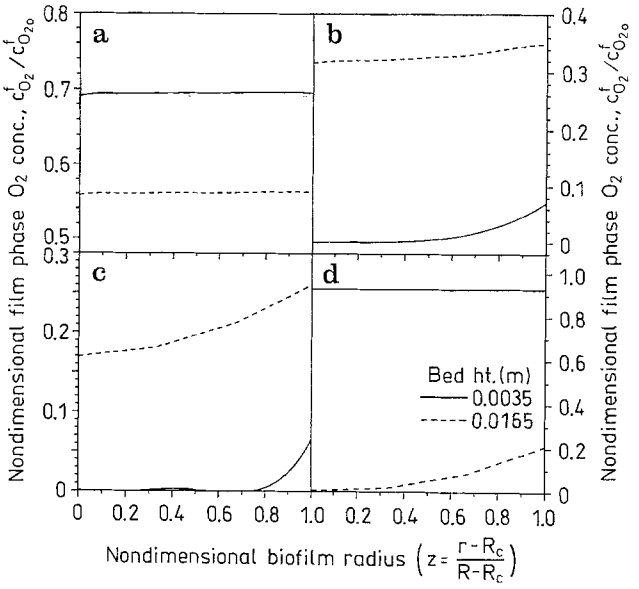

Fig. 5a–d. Film phase oxygen concentration profiles as a function of radius of biofilm around substrate particle at different bed heights for (**a**) $t=15$ h, (**b**) $t=25$ h, (**c**) $t=40$ h, and (**d**) $t=76$ h

concentration profiles are shown for two regions, namely, top region of the bed ($y=0.0035$) and center region ($y=0.0165$) of the bed. During the initial stages of fermentation ($t=15$ h), the region close to the center of the bed ($y=0.0165$) experiences heat build-up in such a way that the temperature rises quite close to 38 °C at which the maximum growth rate occurs. Furthermore, gas phase oxygen concentrations are also high in the entire bed (Fig. 4(b)). Hence the regions close to the center experience better growth and this is reflected by the fact that the oxygen concentrations in the film on the particles situated near the center ($y=0.0165$) are lower than the oxygen concentrations in the film on the particles close to the top ($y=0.0035$). As fermentation proceeds ($t=25$ h), the oxygen concentrations in biofilm at the top region of the bed ($y=0.0035$) is lower than those at the center regions ($y=0.0165$). This observation is contrary to the general expectation that the oxygen concentrations are higher at the top region. The center zone has much higher temperature (Fig. 4(a)) and lower gas phase oxygen concentration (Fig. 4(b)) than those compared to the top of the bed. This results in rapid consumption of oxygen at the top region ($y=0.0035$) as compared to center region ($y=0.0165$). Therefore, film phase oxygen concentration for the biofilm on the particles near the top becomes lower than that in the film on the particles near the center. This trend is also observed at $t=40$ hours. At $t=76$ h, the growth is complete near the top of the bed, and therefore, not much of oxygen is consumed. As a result, the films on the particles near the top get saturated with oxygen whereas the cell growth and oxygen consumption is still taking place near the center. So the oxygen concentration in the films near the center region are still very low. Contrary to the gas phase oxygen concentration which is always higher at the top of the bed as compared to the center of the bed, the oxygen concentration in the biofilm on the particles shows such an oscillatory behavior.

Another interesting observation can be made from Figs. 5(a) through (d). At initial stages of fermentation ($t=15$ h), the biofilm thickness is small, and therefore, the film phase concentration variations with radius are negligible at both bed heights (Fig. 5(a)). At $t=25$ h, the film phase oxygen centrations are not only lower as compared to those at $t=15$ h, but steep gradients within the biofilm can also be seen (Fig. 5(b)). Of particular interest is the oxygen profile near top region, $y=0.0035$. It should be pointed out that oxygen supply is from the top of the bed. Subsequently, the gas phase oxygen concentrations near the top region are farily high (Fig. 5(b)). In spite of high gas phase concentrations, the film phase oxygen concentrations are negligibly small for interior region of the biofilm from $z=0$ to $z=0.75$. In other words, even though aerobic conditions exist in the gas phase, local near anaerobic conditions exist in the expanding biofilm around the particles. This, in turn, can adversely affect the growth of cells and the metabolite produced by the growing cells. Similar phenomena can also be seen at $t=40$, Fig. 5(c). At $t=76$ h, the oxygen consumption decreases in the top region due to stoppage of cell growth and biofilm gets saturated with oxygen. The cell growth continues at the center region leading to lower film phase oxygen concentrations in this region ($y=0.0165$, Fig. 5(d)). Thus, oxygen concentration profiles in the biofilm phase shows oscillatory pattern even though gas phase oxygen concentration decreases monotonically from top to center of the bed.

It is clear from above discussions that heat and mass transfer limitations influence the performance of the solid state fermentation process in tray bioreactor. It is definitely desirable to eliminate the transport limitations in order to achieve optimal performance. Due to simultaneous influence of the temperature and the oxygen concentration on the growth rate of cells, it is difficult to determine which of the two influence the process more strongly. An attempt is made to throw some light on this aspect so that attention can be focused on eliminating the rate controlling limitation. The model simulation is done by assuming either one of the two or both transport limitations are present and height average cell mass density is compared for all cases. The four possibilities are:

(i) No limitation is present, that is, $C_{O_2}(y, t)=C_{O_{2o}}$, $C^f_{O_2}(r, t)=C^f_{O_{2o}}$ for all y, $T(y, t)=T_o$. Only cell mass balance Eq. (3) is considered.

(ii) Only mass transfer limitation is present, that is, $T(y, t)=T_o$. Only oxygen mass balances for gas phase, Eq. (1) and film phase, Eq. (2) and cell mass balance Eq. (3) are considered.

(iii) Only heat transfer limitation is present, that is, $C_{O_2}(y, t)=C_{O_{2o}}$, $C^f_{O_2}(r, t)=C^f_{O_{2o}}$ for all y. Only cell mass balance Eq. (3) and energy balance Eq. (4) is considered.

(iv) Both heat and mass transfer limitations are present. All balance equations, Eqs. (1) through (4), are considered.

Clearly case (iv) is the general case which has been discussed at length earlier. The height average cell mass densities for above four cases are shown in Fig. 6(a). Case (i) predicts simple exponential growth of cells in absence of any limitations. It can be seen from Fig. 6(a) that the cell densities for Case (i) are far away from the that of Case (iv) which reconfirms the earlier obervation that heat and mass transfer

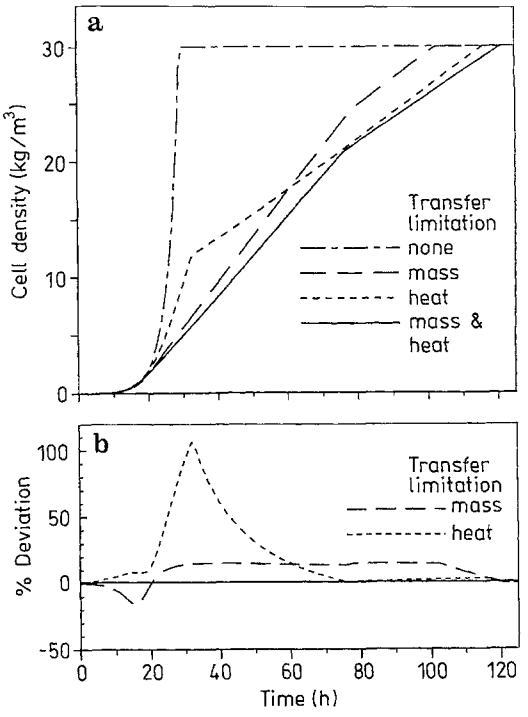

Fig. 6. (a) Cell density and (b) % deviation in cell density variations as function of time under conditions of different transport limitations

limitations play an important role in determining the performance of the tray bioreactor for SSF. Fig. 6(b) shows the % derviation in cell densities for Cases (ii) and (iii) from the cell density for Case (iv). During initial stages of fermentation (till about 20 hours), the cell densities in all four cases is more or less identical which indicates that the heat and mass transfer limitations are not significant in this period. The comparison of cell densities in Case (iii) (mass transfer limitations neglected) and (iv), Fig. 6(b), shows that % deviation is significant at intermediate periods (from $t=20$ to $t=80$ h). In addition the magnitude of % deviation for Case (ii) (heat trasfer limitations neglected) is smaller than that for Case (iii) during this period. These two observations imply that mass transfer limitations are important during intermediate period of fermentation. Beyond 80 hours, % deviations for Case (iii) are negligible while those for Case (ii) are higher in magnitude. This suggests that the mass transfer limitations are not important and heat transfer limitations are crucial in final stages of fermentation.

4 Conclusions

A heterogeneous model is proposed for simulating heat and mass transfer in solid state fermentation process occurring in tray bioreactor. The model incorporates the transport of oxygen in bed of moist substrate particles, simultaneous transport and consumption of oxygen in expanding biofilm around the particle, and heat transport in the bed. The important feature of this model is the incorporation of local transport phenomena within the biofilm phase. Previous models of solid state fermentation does not incorporate this phenomena. The analysis of biofilm expansion around single

particle is carried out to gain some insight into cell growth. The model predicts that oxygen transport limitations under conditions of zero order oxygen consumption kinetics lead to the upper limit of cell density that can be obtained in solid state fermentation. The value of maximum cell density is shown to depend on the gas phase oxygen concentration and the temperature around the biofilm. However, with assumption of first order kinetics for oxygen consumption no such limit is observed. The simulation of the model for tray bioreactor clearly shows the effect of heat and mass transfer limitations on the cell growth. The oxygen concentrations in the expanding biofilm phase show an interesting oscillatory pattern with biofilm at the top of the bed showing less oxygen concentration than those in the center regions during intermediate periods of fermentation. Furthermore, in spite of aerobic conditions existing in the gas phase in the top regions, near anaerobic conditions exist within the biofilm. This can adversely affect the nature of metabolites produced by growing cells. During the initial stages of fermentation, the heat and mass transfer limitations are found to be negligibly small. However, during intermediate stages mass transfer limitations are found to be important while at final stages of fermentation heat transfer limitations dominate the performance of the process. The model developed in this work leads to better understanding of transport limitations and design of bioreactors for solid state fermentation processes. The model, although developed for growth of Aspergillus niger, can easily be extended for growth of other organisms. The effect of other growth limiting substrates, such as carbon source, can easily be incorporated in the model. The work in this direction is currently under progress in our laboratory.

References

1. **Aidoo, K.E.; Hendry, R.; Wood, B.J.B.:** Solid substrate fermentations. Advances in Applied Microbiology. 28 (1980) 201–237
2. **Andre, G.; Moo-Young, M.; Robinson, T.M.:** Improved method for the dynamic measurement of mass transfer coefficient for application to solid-substrate fermentation. Biotechnol. Bioeng. 23 (1981) 1611–1622
3. **Cooney, C.L.; Wang, D.I.C.; Manteles, R.I.:** Measurement of heat evolution and correlation with oxygen consumption during microbialgrowth. Biotechnol. Bioeng. 11 (1968) 269–281
4. **Crank, J.:** Free and Moving Boundary Problems. Oxford University Press, London, 1984
5. **Finger, S.M.; Hatch, R.T.; Regan, T.M.:** Aerobic microbial growth in semisolid matrices: Heat and mass transfer limitation. Biotechnol. Bioeng. 28 (1976) 1193–1218
6. **Finlayson, B.A.:** In: Nonlinear Analysis in Chemical Engineering, McGraw-Hill, New York, 1980
7. **Froment, G.F.; Bischoff, K.B.:** In: Chemical Reactor Design and Analysis, John Wiley & Co., New York, 1979
8. **Georgiou, G.; Shuler, M.L.:** A computer model for the growth and differentiation of a fungal colony on solid substrate. Biotechnol. Bioeng. 28 (1986) 405–416
9. **Hesseltine, C.W.:** Solid state fermentations. Biotechnol. Bioeng. 14 (1972) 517–532
10. **Kobayashi, T.: Van Dedem, G.; Moo-Young, M.:** Oxygen transfer into mycelial pellets. Biotechnol. Bioeng. 15 (1973) 27–45
11. **Laukevics, J.J.; Aspite, A.F.; Viesturs, U.S.; Tengerdy, R.P.:** Steric hindrance of growth of filamentous fungi in solid substrate fermentation of wheat straw. Biotechnol. Bioeng. 27 (1985) 1687–1691
12. **Lonsane, B.K.; Ghildyal, N.P.; Budiatman, S.; Ramakrishna, S.V.:** Engineering aspects of solid state fermentation. J. Enz. Microb. Technol. 7 (1985) 258–265
13. **Mitchell, D.A.; Do, D.D.; Greenfield, P.F.:** A semimechanistic mathematical model for growth of Rhizophus oligosporus in a model solid-state fermentation system. Biotechnol. Bioeng. 38 (1991) 353–362
14. **Perry, R.H.; Chilton, C.H.:** In: Chemical Engineer's Handbook. Fifth Edition, McGraw-Hill, New York, 1973
15. **Raghava Rao, M.K.; Gowthaman, M.K.; Ghildyal, N.P.; Karanth, N.G.:** A mathematical model for solid state fermentation in tray bioreactors. Bioprocess Engineering. 8 (1993) 255–262
16. **Rajagopalan, S.; Modak, J.M.:** Heat and Mass Transfer Simulation Studies for Solid-State Fermentation Processes, Chemical Engineering Science 49 (1994) 2187–2193
17. **Rathbun, B.L.; Shuler, M.L.:** Heat and mass transfer effects in static solid-substrate fermentations: Design of fermentation chambers. Biotechnol. Bioeng. 25 (1983) 929–937
18. **Saucedo-Castaneda, G.; Gutierrez-Rojas, M.; Bacquet, G.; Raimbault, M.; Vibiegra-Gonzalez, G.:** Heat transfer simulation in solid substrate fermentation. Biotechnol. Bioeng. 35 (1990) 802–808
19. **Wittler, R.; Baumgartl, H., Lubbers, D.W.; Schugerl, K.:** Investigations of Oxygen Transfer into Penicillium chrysogenum Pellets by Microprobe Measurements. Biotechnol. Bioeng. 28 (1986) 1024–1036